Polaritons in semiconductor multiple-quantum-well structures with Förster-type interwell coupling

Nguyen Ba An* and Günter Mahler
Institut für Theoretische Physik und Synergetik, Universität Stuttgart, Pfaffenwaldring 57/4, 70550 Stuttgart, Germany
(Received 18 July 1994)

When the barrier potential is high enough and/or its thickness large enough resonance tunneling becomes negligible in multiple-quantum-well structures. In this case a possible mechanism to connect the quantum wells is a Förster-type interwell coupling that originates from the long-range electron-hole exchange interaction. We theoretically investigate excitons in such a coupled multiple-quantum-well structure subject to an external light field, and show that the resulting polaritons behave in a qualitatively different way than those in uncoupled quantum-well structures. Of particular interest are interbranch polariton transitions and the redistribution of the radiative damping rate between different polariton branches. Numerical calculations are performed for a CdS-coupled double-quantum-well structure with dephasing by phonons taken into account.

I. INTRODUCTION

The past two decades have witnessed rapid progress in research and technology of different artificial low-dimensional heterostructures, where quantum-size effects are exploited to produce devices with performance characteristics superior to those of conventional bulk (3D) homostructures. Semiconductor multiple-quantum-well structures (MQWS's) are promising candidates for the latest generation of modern laser and super-high-speed optoelectronic devices.

In a MQWS the wells are coupled: If the barrier potential is not too high and not too wide, the wells are connected by tunneling because the wave functions of the carriers in different wells overlap. In this way, real-space particle transport along the growth direction (z axis) is possible, bringing about a number of attractive phenomena: charge separation induced optical bistability,[1] interwell charge oscillations emitting tunable terahertz radiations,[2–5] barrier-to-well capture and well-to-barrier escape of carriers,[6,7] spin-flip Raman scattering,[8] phonon-assisted resonant magnetotunneling,[9] and relaxation of nonequilibrium electrons,[9] formation of crossed excitons,[11,12] i.e., excitons comprising an electron in one well and a hole in another well, etc.

However, tunneling is not the only mechanism for connecting the wells. In fact, there are phenomena that cannot be explained by tunneling. For example, the diffusion coefficient measurements[13,14] in MQWS's with broad barriers have shown that the diffusion coefficient decreases as a power of barrier width but not exponentially, as expected for tunneling in MQWS's with thin barriers. Tunneling mechanisms are also unable to explain the recent experimental observation[15] of energy transfer between wells separated by thick barriers. One possible mechanism to explain the above-mentioned experimental results (see, e.g., Refs. 16 and 17) would be a Förster-type interwell energy transfer,[18] which occurs via dipole-dipole interaction between excitons and electron-hole pairs residing in different wells. This Förster-type interwell coupling has only recently become of interest for MQWS's,[15–17,19,20] though it is quite familiar in molecular crystals.[21]

In this paper, we deal with the photon-exciton interaction in such a MQWS with Förster-type interwell coupling. The resulting hoppinglike transition of excitons from well to well is taken into account to any order yielding the "true" exciton, which belongs to the whole structure and is delocalized over all wells. The interaction of a bulk photon with such a true MQWS exciton, which is also accounted for in any order, forms a MQWS polariton. This polariton, unlike the bulk one,[22] carries peculiar features of MQWS due to the translational symmetry breaking along the growth direction. For a single-quantum-well structure (SQWS) the polariton concept has been considered recently in Refs. 23–28, where it is shown that for each region of $\Omega(k_\parallel) > k_\parallel$ (Ω and $k_\parallel$ are the polariton energy and its in-plane wave vector, i.e., the wave vector in the plane perpendicular to the growth direction) and for $\Omega(k_\parallel) < k_\parallel$ there is one polariton. We will show that in a coupled MQWS in each of the two above regions there are as many polaritons ("polariton branches") as the number of wells involved. Similar to the SQWS case, in a coupled MQWS, polaritons with energy $\Omega(k_\parallel) > k_\parallel$ possess a finite radiative lifetime whereas those with $\Omega(k_\parallel) < k_\parallel$ are nonradiative. Nevertheless, for light wavelengths λ of interest and typical well widths l of experimentally investigated samples ($\lambda \simeq 500$–800 nm, $l \simeq 5$–20 nm) the polariton in a SQWS is almost independent of the well width,[23] while both the polariton dispersion and damping in a coupled MQWS are sensitive to the structure parameters. If interwell coupling is ignored, the polariton in each well has nearly equal radiative damping independent of the well width. But when the coupling between wells comes into play, a "redistribution" of damping between the polariton branches results: a lower branch gets a shorter radiative lifetime than an upper branch does, and this difference in the lifetime is larger for stronger interwell coupling.

Our paper is organized as follows. In Sec. II, we derive from an original interacting electron-hole picture the exciton Hamiltonian with taking into account both in-

trawell and interwell electron-hole Coulomb-exchange interaction. The long-range electron-hole exchange interaction between wells results in the appearance of hoppinglike nondiagonal terms in the exciton-exciton interaction Hamiltonian which is diagonalized to yield the so-called true exciton. This true exciton is then to be coupled to the photon field in Sec. III where a system of equations is established, the numerical solution of which gives the $k_{\parallel}$ dependence of both energy and radiative damping of the multibranch polariton. Section IV calculates the rate of polariton scattering by phonons and compares this with the radiative one obtained in Sec. III. Finally, our paper ends with a short discussion and conclusion. We use throughout this paper units with $\hbar=c=1$, where $\hbar$ and c are, respectively, the Planck constant and the speed of light in vacuum.

II. TRUE EXCITONS

Let us consider a general MQWS in which the wells have widths l_n and their spatial separations in the growth direction are $d_{nn'}$ ($d_{nn'}=d_{n'n}$). The motion in the xy plane, i.e., the plane perpendicular to the growth direction (z direction), is free, whereas that along the z direction is quantum confined. To lowest order in the effective-mass approximations and according to the envelope function theory, the normalized one-carrier wave function within a well can be constructed as a product of a plane wave with in-plane wave vector $\mathbf{k}_{\parallel}$ multiplied by the 3D Bloch function $u_{\alpha}(\mathbf{r})$ [α denotes electron (e) or hole (h) in the two-band case] at the band extrema and the carrier envelope function $\phi_{\alpha}^{(n)}(z)$ in the z direction:

$$\psi_{\alpha k_{\parallel}}^{(n)}(\mathbf{r})=\frac{1}{\sqrt{L_x L_y}}e^{i\mathbf{k}_{\parallel}\rho_{\parallel}}u_{\alpha}(\mathbf{r})\phi_{\alpha}^{(n)}(z)\ . \tag{1}$$

In (1), $L_x L_y$ is the area of periodicity in the xy plane, $\mathbf{r}=(\boldsymbol{\rho}_{\parallel},z)$, and

$$\phi_{\alpha}^{(n)}(z)=\left[\frac{2}{l_n}\right]^{1/2}\cos\left[\frac{\pi z}{l_n}\right] \tag{2}$$

is the α-independent envelope function in well n for the case of the infinite barrier potential, when only the lowest electron (highest hole) subband is considered. Taking (1) as a basic set, we can derive the Hamiltonian of the electron-hole system of the MQWS in second quantization as (operators e and e^{+} stand for the electron while h and h^{+} for the hole)

$$\begin{aligned}H_{eh}=&\sum_{n\mathbf{k}_{\parallel}s}[\varepsilon_{en}(k_{\parallel})e_{n\mathbf{k}_{\parallel}s}^{+}e_{n\mathbf{k}_{\parallel}s}+\varepsilon_{hn}(k_{\parallel})h_{n\mathbf{k}_{\parallel}s}^{+}h_{n\mathbf{k}_{\parallel}s}]+\tfrac{1}{2}\sum_{\mathbf{p}_{\parallel}\mathbf{q}_{\parallel}\mathbf{k}_{\parallel}}\sum_{nn'ss'}C_{nn'}(k_{\parallel},d_{nn'})\\&\times[e_{n\mathbf{p}_{\parallel}s}^{+}e_{n'\mathbf{q}_{\parallel}s'}^{+}e_{n'\mathbf{q}_{\parallel}+\mathbf{k}_{\parallel}s'}e_{n\mathbf{p}_{\parallel}-\mathbf{k}_{\parallel}s}+h_{n\mathbf{p}_{\parallel}s}^{+}h_{n'\mathbf{q}_{\parallel}s'}^{+}h_{n'\mathbf{q}_{\parallel}+\mathbf{k}_{\parallel}s'}h_{n\mathbf{p}_{\parallel}-\mathbf{k}_{\parallel}s}-2e_{n\mathbf{p}_{\parallel}s}^{+}h_{n'\mathbf{q}_{\parallel}s'}^{+}h_{n'\mathbf{q}_{\parallel}+\mathbf{k}_{\parallel}s'}e_{n\mathbf{p}_{\parallel}-\mathbf{k}_{\parallel}s}]\\&+\sum_{\mathbf{p}_{\parallel}\mathbf{q}_{\parallel}\mathbf{k}_{\parallel}}\sum_{nn'ss'\sigma}X_{\sigma,nn'}(k_{\parallel},d_{nn'})[e_{n\mathbf{k}_{\parallel}-\mathbf{p}_{\parallel}s}^{+}h_{n\mathbf{p}_{\parallel}s}^{+}h_{n'\mathbf{q}_{\parallel}s'}e_{n'\mathbf{k}_{\parallel}-\mathbf{q}_{\parallel}s'}]\ ,\end{aligned} \tag{3}$$

where $s,s'=\pm\frac{1}{2}$ denote the carrier spin projection and

$$\varepsilon_{\alpha n}(k_{\parallel})=E_g(1-\delta_{\alpha h})+\frac{1}{2m_{\alpha}}\left[k_{\parallel}^2+\frac{\pi^2}{l_n^2}\right]\ , \tag{4}$$

with m_{α} the carrier effective mass which is n independent if all wells are assumed to be of the same material and, E_g the band gap of the well material. The Coulomb interaction reads

$$C_{nn'}(k_{\parallel},d_{nn'})=\frac{2\pi e^2}{\epsilon L_x L_y k_{\parallel}}\exp[-k_{\parallel}d_{nn'}(1-\delta_{nn'})]\ , \tag{5}$$

with e the electron charge and ϵ an average dielectric constant neglecting any difference between the dielectric properties of the well and the barrier. The electron-hole exchange interaction reads

$$\begin{aligned}X_{\sigma,nn'}(k_{\parallel},d_{nn'})=&\left[S_{3D}I_n\delta_{\sigma S}+\frac{2\pi\mu^2 k_{\parallel}}{\epsilon L_x L_y}J_n(k_{\parallel})(1-\delta_{\sigma S})(1-\delta_{\sigma T})(\delta_{\sigma L}-\delta_{\sigma Z})\right]\delta_{nn'}\\&+\frac{2\pi\mu^2 k_{\parallel}}{\epsilon L_x L_y}e^{-k_{\parallel}d_{nn'}}K_n K_{n'}^{*}(1-\delta_{nn'})(1-\delta_{\sigma S})(1-\delta_{\sigma T})(\delta_{\sigma L}-\delta_{\sigma Z})\ ,\end{aligned} \tag{6}$$

with $\sigma=S$ denoting the intrawell short-range interaction and $\sigma=L$, Z, T denoting the long-range interactions for the L,Z, and T polarization, respectively. For the L polarization, the dipole moment

$$\mu=\frac{e}{v_0}\int_{v_0}d\xi u_e^{*}(\xi)\xi u_h(\xi)\ , \tag{7}$$

lies in the xy plane and is parallel to $\mathbf{k}_{\parallel}$ (v_0 is the unit-cell

volume and ζ is a coordinate vector within a unit cell). For the T polarization, μ also lies in the xy plane but is perpendicular to $\mathbf{k}_\parallel$, while for the Z polarization μ is in the z direction. In (6), S_{3D} expresses the 3D electron-hole exchange integral,

$$S_{3D}=\frac{e^2}{\epsilon v_0}\int_{v_0}d\xi_1\int_{v_0}d\xi_2\frac{u_e^*(\xi_1)u_h^*(\xi_1)u_h(\xi_2)u_e(\xi_2)}{|\xi_2-\xi_1|}\ , \tag{8}$$

which is enhanced in the confinement regime by the factor I_n,

$$I_n=\int_{-l_n/2}^{l_n/2}dz\,|\phi^{(n)}(z)|^4\ . \tag{9}$$

For an infinite barrier potential, $I_n=\frac{3}{2}$. The intrawell long-range exchange interaction described by the second term in the square parentheses of (6) depends on $k_\parallel$ explicitly and via $J_n(k_\parallel)$ implicitly, where

$$J_n(k_\parallel)=\int_{-l_n/2}^{l_n/2}dz\int_{-l_n/2}^{l_n/2}dz'e^{-k_\parallel z}|\phi^{(n)}(z')\phi^{(n)}(z+z')|^2\ . \tag{10}$$

For an infinite barrier potential, we find

$$J_n(k_\parallel)=\frac{(3k_\parallel^2l_n^2+8\pi^2)(1-e^{-k_\parallel l_n})}{2k_\parallel l_n(k_\parallel^2l_n^2+4\pi^2)}\ , \tag{11}$$

which tends to unity for $k_\parallel l_n\ll 1$ and to $3/(2k_\parallel l_n)$ for $k_\parallel l_n\gg 1$. Therefore, for large $k_\parallel$ the intrawell long-range exchange interaction becomes independent of $k_\parallel$, for large l_n it tends to vanish, and for $k_\parallel=0$ it is degenerate for the all three polarizations. This latter fact is a surprising feature caused by reduced dimensionality, and should be contrasted with the bulk situation, where at $k_\parallel=0$ no such degeneracy occurs.[24] The last term in (6) is the Förster-type interwell coupling, which is of long-range character and depends on both $k_\parallel$ and $d_{nn'}$. K_n is given by

$$K_n=\int_{-l_n/2}^{l_n/2}dz\,|\phi^{(n)}(z)|^2\ , \tag{12}$$

which equals unity for finite barrier potential. Note that in deriving the above formulas we have neglected tunneling and used the multipole expansion up to the second order in $|\xi_2-\xi_1|/|\mathbf{R}_2-\mathbf{R}_1|$ (ξ_i is the radius vector of carrier i within a unit cell of position $\mathbf{R}_i$).

To get the exciton Hamiltonian from (3), we realize that an exciton is in fact a bound electron-hole pair. The electron and the hole in the exciton may reside within the same well or in different wells.[11,12] When tunneling is ignored only the former situation is possible. Furthermore, because the electron and the hole have a spin $\frac{1}{2}$ each, the exciton basic state vector in the absence of spin-orbit coupling should transform according to a representation of the rotation group, which is the direct product $D_{1/2}\otimes D_{1/2}$ of the two representations $D_{1/2}$ where $D_{1/2}$ is the bidimensional irreducible representation of the rotation group of a spin-$\frac{1}{2}$ particle. In accordance with group theory, any exciton may be classified into two classes: the so-called paraexcitons, which have total spin $J=0$ and projection $J_z=0$, and the so-called orthoexcitons, which have $J=1$ and $J_z=0,\pm1$. The exciton operator is then in second quantization,

$$b^+_{\nu n\mathbf{k}_\parallel JJ_z}=\frac{1}{\sqrt{L_xL_y}}\sum_{\mathbf{p}_\parallel s}\chi_\nu(\mathbf{p}_\parallel-\eta_h\mathbf{k}_\parallel)A^J_{s,J_z-s}\times K_n e^+_{n\mathbf{k}_\parallel-\mathbf{p}_\parallel s}h^+_{n\mathbf{p}_\parallel J_z-s}\ , \tag{13}$$

where $\eta_h=m_h/(m_e+m_h)$, χ_ν describes the relative motion of the electron-hole pair constituting the exciton in a quantum state ν, and A^J_{s,J_z-s} are the Clebsch-Gordan coefficients. Assuming an infinite barrier potential ($K_n=1$), Eq. (13) represents a strict 2D exciton creation operator. Making use of the othonormalization conditions of χ_ν and A^J_{s,J_z-s}, we are able to inverse (13) as (for simplicity only the lowest exciton state is studied: the index ν can then be dropped)

$$e^+_{n\mathbf{p}_\parallel s}h^+_{n\mathbf{q}_\parallel s'}=\frac{1}{\sqrt{L_xL_y}}\sum_J\chi^*_\nu(\eta_e\mathbf{q}_\parallel-\eta_h\mathbf{p}_\parallel)\times A^{J*}_{s,s'}b^+_{n\mathbf{p}_\parallel+\mathbf{q}_\parallel J_{s+s}}\ , \tag{14}$$

with $\eta_e=1-\eta_h$. At low excitation levels, we can limit ourselves to the one-electron and one-hole subspaces. Then following the "excitonization technique" applied in Refs. 29–31 and observing

$$\sum_s A^J_{s,-s}=\sum_s A^{J*}_{s,-s}=\sqrt{2}\delta_{J0}\ , \tag{15}$$

$$\sum_{ss'}A^{J*}_{s,s'}A^J_{s,s'}=\delta_{JJ'}\ , \tag{16}$$

we arrive at the exciton Hamiltonian of the form

$$H_{\rm exc}=\sum_{n\mathbf{p}_\parallel}\left\{\sum_{J_z=0,\pm1}E_n^{(S)}(p_\parallel)O^+_{n\mathbf{p}_\parallel J_z}O_{n\mathbf{p}_\parallel J_z}+\sum_{\sigma=L,Z,T}\left[E_n^{(\sigma)}(p_\parallel)P^{(\sigma)}_{n\mathbf{p}_\parallel}+P^{(\sigma)}_{n\mathbf{p}_\parallel}+\sum_{n'\neq n}F^{(\sigma)}_{nn'}(p_\parallel,d_{nn'})\times P^{(\sigma)+}_{n\mathbf{p}_\parallel}P^{(\sigma)}_{n'\mathbf{p}_\parallel}\right]\right\}\ . \tag{17}$$

In (17), we have identified

$$O_{n,\mathbf{p}_\parallel J_z}\equiv b_{n\mathbf{p}_\parallel J=1J_z} \tag{18}$$

as the orthoexciton, and

$$P^{(\sigma)}_{n\mathbf{p}_\parallel}\equiv b^{(\sigma)}_{n\mathbf{p}_\parallel J=0J_z=0} \tag{19}$$

as the paraexciton of σ polarization ($\sigma=L,Z,T$). The other quantities in (17) are given by [in (21), $\sigma=L,Z$, while in (20), σ includes also S and T]

$$E_n^{(\sigma)}(p_\parallel)=E_g+\frac{p_\parallel^2}{2(m_e+m_h)}+\frac{\pi^2}{2m_{eh}l_n^2}-4\mathrm{Ry}+2L_xL_yX^{(\sigma)}_{nn}(p_\parallel)|\Phi_{2D}(0)|^2\ , \tag{20}$$

$$F_{nn'}^{(\sigma)}(p_\parallel,d_{nn'})=2L_xL_yX_{nn'}^{(\sigma)}(p_\parallel,d_{nn'})|\Phi_{2D}(0)|^2 , \quad (21)$$

with $m_{eh}=m_em_h/(m_e+m_h)$, Ry the 3D Rydberg, $\Phi_{2D}(0)=2\sqrt{2}/(\sqrt{\pi}a_B)$ the real-space exciton envelope function at the origin, and a_B the 3D Bohr radius. From (17), we see that the interwell hoppinglike (i.e., Förster-type) terms, which are proportional to $F_{nn'}^{(\sigma)}(n\neq n')$, appear from the long-range electron-hole exchange interaction, i.e., from the last multiple sum in (3). The exciton now can hop from well to well and by this energy can be transferred from well to well, too. However, such a kind of energy transfer does not mean a real-space escape of exciton between wells, i.e., a free-carrier transfer itself or transfer of excitons as a whole.[32] Without tunneling, the exciton remains completely confined in one well. Yet, thanks to the Förster-type coupling the energy of annihilation of an exciton in one well, say, well n, can be "utilized" to create another exciton in any other well, say, well n', which can be far from the initial well n. Such virtual hoppings connect all wells of the MQWS and one can no longer distinguish an individual well. Since $X_{nn'}^{(T)}=0$ $(n\neq n')$, neither orthoexcitons nor paraexcitons with T polarization participate in hopping. So, being interested in the hopping mechanism, we are left with the paraexciton with L and Z polarization only. For a given polarization, we can suppress the index σ and, to further simplify notations without loss of generality, we have chosen to treat a double-quantum-well structure (DQWS), the Hamiltonian of which reads

$$H=E_1(p_\parallel)P_{1\mathbf{p}_\parallel}^+P_{1\mathbf{p}_\parallel}+E_2(p_\parallel)P_{2\mathbf{p}_\parallel}^+P_{2\mathbf{p}_\parallel} +F(p_\parallel,d)[P_{1\mathbf{p}_\parallel}^+P_{2\mathbf{p}_\parallel}+P_{2\mathbf{p}_\parallel}^+P_{1\mathbf{p}_\parallel}] . \quad (22)$$

Here, $F\equiv F_{12}=F_{21}$ and $d\equiv d_{12}=d_{21}$. In the next section, we will couple the exciton to an external light field. The phonon does not distinguish between the wells and interacts with the eigenstates of the coupled DQWS rather than with individual excitons in separate wells. In this case, the eigenstate of the coupled DQWS can be obtained by taking into account the interwell interaction to all orders. This is done by the following transformation:

$$P_{n\mathbf{p}_\parallel}=\sum_\nu u_{n\nu}(p_\parallel,d)B_{\nu\mathbf{p}_\parallel}, \quad \nu=1,2 \quad (23)$$

where the coefficients $u_{n\nu}$ are determined as

$$u_{n\nu}(p_\parallel,d)=\alpha_{n\nu}\left\{\frac{F^2(p_\parallel,d)}{[E_n(p_\parallel)-\mathcal{E}_\nu(p_\parallel,d)]^2+F^2(p_\parallel,d)}\right\}^{1/2} , \quad (24)$$

with $\alpha_{11}=\alpha_{22}=\alpha_{12}=-\alpha_{21}=1$ chosen to recover the uncoupled situation when the hopping disappears, i.e., $B_\nu\to P_\nu$ when $F\to 0$. The Hamiltonian (22) is now diagonal in B operators,

$$H=\sum_{\nu\mathbf{p}_\parallel}\mathcal{E}_\nu(p_\parallel,d)B_{\nu\mathbf{p}_\parallel}^+B_{\nu\mathbf{p}_\parallel} , \quad (25)$$

with

$$\mathcal{E}_\nu(p_\parallel,d) =\tfrac{1}{2}\{E_1(p_\parallel)+E_2(p_\parallel) +(-1)^\nu\sqrt{[E_2(p_\parallel)-E_1(p_\parallel)]^2+4F^2(p_\parallel,d)}\} . \quad (26)$$

$\mathcal{E}_\nu$ and $B_\nu(B_\nu^+)$ describe the elementary excitation of the coupled DQWS, which we refer to as "true" excitons. As a rule, these true excitons belong to the whole structure and are delocalized over the two wells. Within this unified picture it makes no sense to speak of "left well," "right well," "narrow well," or "wide well," etc. It is these true excitons to which the light will be coupled in the next section.

III. POLARITONS

The optical properties of a material are mainly determined by the interaction of photons with the respective elementary excitations. In semiconductors the photon-exciton interaction is always of central interest. In bulk crystals the translational symmetry implies that each $\mathbf{k}$ exciton is converted into only one-photon mode with precisely the same wave vector $\mathbf{k}$, and vice versa. Hence, the corresponding eigenmode, the polariton, is stable and cannot decay, unless other kinds of interaction are added. When the dimensionality is reduced, however, the symmetry is reduced too, and the selection rule becomes eroded. In quantum-well structures, breakdown of the translational symmetry in the growth direction causes serious consequences in many physical phenomena, in particular, for the stability of polariton. Here, in quantum wells, an exciton with $\mathbf{k}_\parallel$ is allowed to interact with an infinite number of photon modes characterized by $\mathbf{q}=(\mathbf{q}_\parallel,\mathbf{q}_\perp)$, where $\mathbf{q}_\parallel=\mathbf{k}_\parallel$ but $\mathbf{q}_\perp$ is arbitrary. This arbitrariness of $\mathbf{q}_\perp$ defines a continuum to which the quantum-well exciton is coupled. This is the physical reason why the polariton in quantum wells can be radiatively unstable even without any anharmonicity.

To show this in detail, let us start from the interaction between photons and quantum-well carriers,

$$H_{\rm int}=-\frac{e}{m}\sum_{n\mathbf{k}\mathbf{k}_\parallel\mathbf{p}_\parallel s}\left[\frac{2\pi}{\epsilon L_xL_yL_zk}\right]^{1/2}(\mathbf{e}\boldsymbol{\Pi}_n) \times[e_{n\mathbf{k}_\parallel-\mathbf{p}_\parallel s}^+h_{nn\mathbf{p}_\parallel-s}^+c_{\mathbf{k}}+\text{H.c.}] . \quad (27)$$

In (27), m is the free-electron mass, L_z is the z direction periodic length for the photon, $\mathbf{e}\equiv\mathbf{e}_{\mathbf{k}}(c_{\mathbf{k}})$ is the photon unit polarization vector (annihilation operator) and, $\boldsymbol{\Pi}_n$ is the interband matrix element of the momentum operator in well n. We now again apply (14) and the excitonization technique.[29–31] With the sum over s giving $\sqrt{2}\delta_{J0}$ (i.e., only paraexcitons are coupled to phonons), the sum over $\mathbf{p}_\parallel$ yielding $L_xL_y\Phi_{2D}(0)$, and with $\boldsymbol{\Pi}_n$ replaced by $-imE_n\boldsymbol{\mu}/e$, (27) finally reads

$$H_{\rm int}=\sum_{n\mathbf{k}_\parallel\mathbf{k}_\perp} g_n(k_\parallel,k_\perp)[c_{\mathbf{k}}^+P_{n\mathbf{k}_\parallel}-P_{n\mathbf{k}_\parallel}^+c_{\mathbf{k}}]\ . \tag{28}$$

Here,

$$g_n(k_\parallel,k_\perp)=2i\left[\frac{\pi}{\epsilon L_z k}\right]^{1/2}(\mathbf{e}\boldsymbol{\mu})E_n(k_\parallel)\Phi_{\rm 2D}(0)G_n(k_\perp)\ , \tag{29}$$

with

$$G_n(k_\perp)=\int_{-l_n/2}^{l_n/2}dz\,|\phi^{(n)}(z)|^2e^{ik_\perp z}\ . \tag{30}$$

For an infinite barrier potential, (30) is evaluated as

$$G_n(k_\perp)=\frac{8\pi^2\sin(k_\perp l_n/2)}{k_\perp l_n(4\pi^2-k_\perp^2l_n^2)}\ , \tag{31}$$

which tends to unity for $k_\perp l_n\to 0$. Note that in (28) we again have dropped the polarization index σ for brevity. Next, when (23) is used in (28), we get the photon-true exciton interaction Hamiltonian, which for a DQWS is of the form

$$H_{\rm int}=\sum_{\nu\mathbf{k}_\parallel\mathbf{k}_\perp} f_\nu(k_\parallel,k_\perp,d)[c_{\mathbf{k}}^+B_{\nu\mathbf{k}_\parallel}-B_{\nu\mathbf{k}_\parallel}^+c_{\mathbf{k}}],\quad \nu=1,2\ , \tag{32}$$

where

$$f_\nu(k_\parallel,k_\perp,d)=\sum_n g_n(k_\parallel,k_\perp)u_{n\nu}(k_\parallel,d),\quad n=1,2\ . \tag{33}$$

The Heisenberg equations of motion for the photon-true exciton system are written as

$$i\dot B_{\nu\mathbf{k}_\parallel}=\mathcal{E}_\nu(k_\parallel,d)B_{\nu\mathbf{k}_\parallel}-\sum_{\mathbf{k}_\parallel}f_\nu(k_\parallel,k_\perp,d)c_{\mathbf{k}}\ , \tag{34}$$

$$i\dot c_{\mathbf{k}}=kc_{\mathbf{k}}+\sum_{\nu'}f_{\nu'}(k_\parallel,k_\perp,d)B_{\nu'\mathbf{k}_\parallel},\quad \nu'=1,2\ . \tag{35}$$

As discussed at the beginning of this section, the sum over $\mathbf{k}_\perp$ in (34) will be of crucial importance in treating quantum-well polaritons. To solve for the eigenmode problem, we transform from the exciton and the photon to the polariton as follows ($\mathcal{B}$ and $\mathcal{B}^+$ stand for polaritons):

$$B_{\nu\mathbf{k}_\parallel}=\sum_\alpha x_{\nu\alpha}(k_\parallel,d)\mathcal{B}_{\alpha\mathbf{k}_\parallel}\ , \tag{36}$$

$$c_{\mathbf{k}}=\sum_\alpha y_\alpha(k,d)\mathcal{B}_{\alpha k_\parallel}\ , \tag{37}$$

where $x_{\nu\alpha}$ and y_α are functions yet to be determined. Requiring $\mathcal{B}$ and $\mathcal{B}^+$ to be operators of the system eigenmode with the eigenvalue Ω yields the following set of equations:

$$\Omega x_{\nu\alpha}(k_\parallel,d)=\mathcal{E}_\nu(k_\parallel,d)x_{\nu\alpha}(k_\parallel,d)-\sum_{\mathbf{k}_\perp}f_\nu(k_\parallel,k_\perp,d)y_\alpha(k,d)\ , \tag{38}$$

$$\Omega y_\alpha(k,d)=ky_\alpha(k,d)=\sum_{\nu'}f_{\nu'}(k_\parallel,k_\perp,d)x_{\nu'\alpha}(k_\parallel,d)\ . \tag{39}$$

Using (39) to replace y_α in (38), we get the equations for $x_{\nu\alpha}$,

$$[\Omega-\mathcal{E}_1(k_\parallel,d)+R_{11}(k_\parallel,\Omega,d)]x_{1\alpha}(k_\parallel,d)+R_{12}(k_\parallel,\Omega,d)x_{2\alpha}(k_\parallel,d)=0\ , \tag{40}$$

$$R_{21}(k_\parallel,\Omega,d)x_{1\alpha}(k_\parallel,d)+[\Omega-\mathcal{E}_2(k_\parallel,d)+R_{22}(k_\parallel,\Omega,d)]x_{2\alpha}(k_\parallel,d)=0\ . \tag{41}$$

The $R_{\nu\nu'}$ are defined as

$$R_{\nu\nu'}(k_\parallel,\Omega,d)\sum_{\mathbf{k}_\perp}\frac{f_\nu(k_\parallel,k_\perp,d)f_{\nu'}(k_\parallel,k_\perp,d)}{\Omega-k}=\sum_{nn'}u_{n\nu}(k_\parallel,d)u_{n'\nu'}(k_\parallel,d)\times\Xi_{nn'}(k_\parallel)Q(k_\parallel,\Omega)\ , \tag{42}$$

where use of (31) and (27) has been made and

$$\Xi_{nn'}(k_\parallel)=-2\mu^2\Phi_{\rm 2D}^2(0)E_n(k_\parallel)E_{n'}(k_\parallel)\ , \tag{43}$$

while

$$Q(k_\parallel,\Omega)=\int_0^\infty\frac{(\mathbf{e}\cdot\boldsymbol{\mu}_0)^2}{k(\Omega-k)}d\mathbf{k}_\perp,\quad \boldsymbol{\mu}_0=\boldsymbol{\mu}/\mu\ . \tag{44}$$

The integral (44) derives from the usual replacement

$$\frac{2\pi}{L_z}\sum_{\mathbf{k}_\perp}\to\int_0^\infty d\mathbf{k}_\perp\ . \tag{45}$$

Nontrivial solutions for (40) and (41) result if

$$[\Omega-\mathcal{E}_1(k_\parallel,d)+R_{11}(k_\parallel,\Omega,d)]\times[\Omega-\mathcal{E}_2(k_\parallel,d)+R_{22}(k_\parallel,\Omega,d)]=R_{12}^2(k_\parallel,\Omega,d)\ . \tag{46}$$

For uncoupled wells the right-hand side (rhs) of (46) is zero, so that an analytical solution can then be found[23] (see also Refs. 25 and 26 where the SQWS solution is obtained by means of Maxwell equations with a suitable nonlocal response function for the electric susceptibility). For coupled wells an analytical solution is impossible even for a DQWS as specified in (46). However, Eq. (46) can be solved semianalytically in the sense that we first carry out exact integration for Q defined by (44) and then use the result in (46) for a subsequent numerical calculation.

At this moment it is necessary to have a closer look at the polarization situations of interest, $\sigma=L$ and Z. As $\mathbf{e}\perp\mathbf{k}$, we have

$$\langle(\mathbf{e}\boldsymbol{\mu}_0)^2\rangle=\frac{k_\perp^2}{2k^2}\ , \tag{47}$$

for $\sigma=L$ and

$$\langle(\mathbf{e}\boldsymbol{\mu}_0)^2\rangle=\frac{k_\parallel^2}{2k^2} \tag{48}$$

for $\sigma=z$, where $\langle\ \rangle$ means an angular average. Using

$\langle(e\mu_0)^2\rangle$ instead of $(e\mu_0)^2$, we can integrate (44) exactly to get

$$Q(k_\parallel,\Omega)=\frac{1}{\Omega}\left[\frac{\pi}{2\Omega}(\sqrt{k_\parallel^2-\Omega^2}-k_\parallel)-1\right] \tag{49}$$

for $\sigma=L$ and

$$Q(k_\parallel,\Omega)=\frac{1}{\Omega}\left[\frac{\pi k_\parallel}{2\Omega}\left[1-\frac{k_\parallel}{\sqrt{k_\parallel^2-\Omega^2}}\right]+1\right] \tag{50}$$

for $\sigma=Z$. From (49) and (50) it follows that Q is real for $\Omega<k_\parallel$ and complex for $\Omega>k_\parallel$. A complex Q being used in (46) via $R_{\nu\nu'}$ adds an imaginary part to Ω, which is nothing else but the radiative decay rate Γ of the polariton. Note that this mathematical reason of the appearance of polariton radiative damping comes here in a quite natural way without assuming $\Gamma\ll\Omega$. Such an assumption has often been made in the literature because this allows application of the formula $1/(z-a\pm i0)=\mathcal{P}[1/(z-a)]\mp\delta(z-a)$. In fact we do not use this formula, and the assumption of $\Gamma\ll\Omega$ is not so good here, especially for the Z polarization, as will be seen later. The physical reasoning at the beginning of this section is of course more convincing.

Another figure of merit of our semianalytic approach is that (49) and (50) also establish a mathematical criterion for the stability of polariton: the condition $\Omega=k_\parallel$ separates radiatively unstable and stable polaritons. We now explain this criterion physically. The finite radiative decay rate of a polariton means that the polariton has a finite probability to be converted into the photon outside the sample, if energy allows. Since outside the sample the photon energy is $\omega=k=\sqrt{k_\parallel^2+k_\perp^2}$, the energy conservation allowing real polariton-to-photon conversion implies

$$\Omega=\omega\equiv\sqrt{k_\parallel^2+k_\perp^2}\ . \tag{51}$$

From (51) it is clear that for $\Omega>k_\parallel$, there are real $k_\perp$ that satisfy (51) and the photon can leave the sample: the polariton is damped radiatively. On the other hand, if $\Omega<k_\parallel$, no real $k_\perp$ can fulfill the energy conservation (51), and thus the real polariton-to-photon conversion is forbidden energetically: the polariton is radiatively undamped.

From Sec. II, we know that the efficiency of interwell hopping depends on barrier width d, well widths l_n and also on well material parameters. It is more efficient for stronger hopping strength F and smaller energy difference $\Delta E=|E_2-E_1|$ (we only deal with a DQWS here). Therefore, using (20), (21), and the relation

$$\mu^2=\frac{\epsilon\Delta_{\rm LT}}{4\pi|\Phi_{\rm 3D}(0)|^2}\ , \tag{52}$$

with $\Delta_{\rm LT}$ being the 3D exciton longitudinal-transverse splitting, $\Phi_{\rm 3D}(0)=1/\sqrt{\pi a_B^3}$ the 3D real-space exciton envelope function at the origin, we can factorize the hopping efficiency $h_{\rm eff}$ as

$$h_{\rm eff}={\rm const}h_{\rm mat}h_{\rm struc}\ . \tag{53}$$

In (53), $h_{\rm mat}=\epsilon\Delta_{\rm LT}a_B m_{eh}/m$ characterizes dependence on the well material parameters while $h_{\rm struc}$ is a factor characterizing dependence on the geometry of the heterostructure which, can be tailor made. For CdS material parameters ($\epsilon=8$, $m_e/m=0.198$, $m_h/m=0.782$, $E_g=2.58$ eV, $\Delta_{\rm LT}=2$ meV, and $a_B=3$ nm) $h_{\rm max}=75.8384$ meV Å, whereas for GaAs this quantity equals 6.9981 meV Å. We have thus chosen CdS for our numerical calculation.

The numerical results for solving Eq. (46) is represented in Figs. 1–8. Figure 1 shows dispersions of the L polariton, for a CdS coupled DQWS with $l_1=13$ nm, $l_2=7$ nm and $d=10$ nm. The two radiatively damped polaritons are drawn by solid curves on the left-hand side (lhs) of the curve $\Omega=k_\parallel$ and those two undamped ones by short-dashed curves on the rhs of $\Omega=k_\parallel$. They "continuously" cross the curve $\Omega=k_\parallel$ because Q in (49) has no singularity. The damping of the lhs polariton branches depends on $k_\parallel$ but must vanish at $k_\parallel=\Omega$ to match the rhs ones. This is seen in Fig. 2, where the lower polariton branch gets more damping than the upper one. The uncoupled wells calculation (not shown) yields practically the same dispersions as in Fig. 1 because here, $\Delta l\equiv|l_2-l_1|=6$ nm is quite large resulting in weak hopping. Furthermore, the damping in the case of uncoupled wells (not shown either) does not feel the difference in well widths: both wells, though with different widths, possess the same damping,[23] which is here close to the solid curve in Fig. 2. The interwell coupling, thus, "splits" the damping in the uncoupled wells case and "redistributes" it so that the lower branch gets a larger damping rate. All this is exhibited more pronouncedly for smaller Δl, as shown in Figs. 3 and 4, where $\Delta l=0.1$ nm. The dispersions are now modified strongly (Fig. 3) as

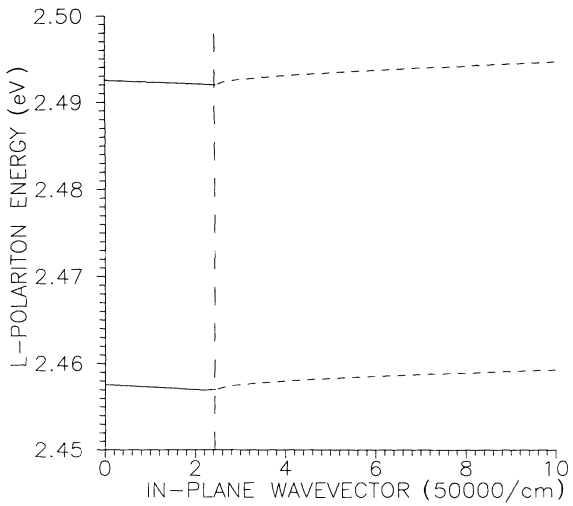

FIG. 1. L-polariton energy, in eV, versus in-plane wave vector $k_\parallel$, in units of 5×10^4 cm^{-1}, for a CdS coupled DQWS with well widths $l_1=13$ nm, $l_2=7$ nm and barrier width $d=10$ nm. The vertical long-dashed line is the curve of $\Omega=k_\parallel$. The solid curves on the lhs of $\Omega=k_\parallel$ are the dispersions of radiatively damped polaritons, while the short-dashed curves on the rhs of $\Omega=k_\parallel$ are those of undamped polaritons.

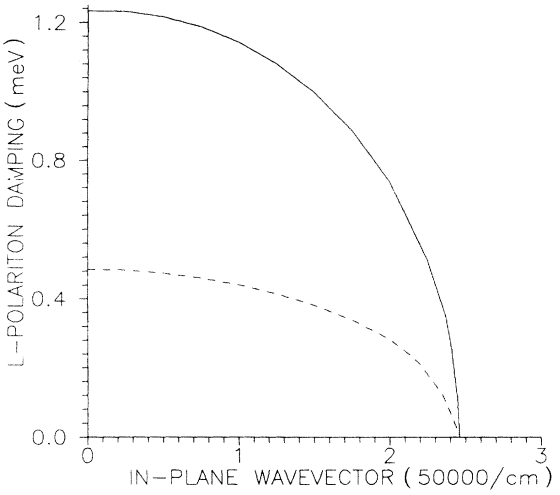

FIG. 2. L-polariton damping, in meV, versus in-plane wave vector $k_{\|}$, in units of 5×10^{4} cm^{-1}, for a CdS coupled DQWS with well widths $l_1=13$ nm, $l_2=7$ nm, and $d=10$ nm. The solid (dashed) curve is for the lower-branch (upper-branch) polariton in Fig. 1.

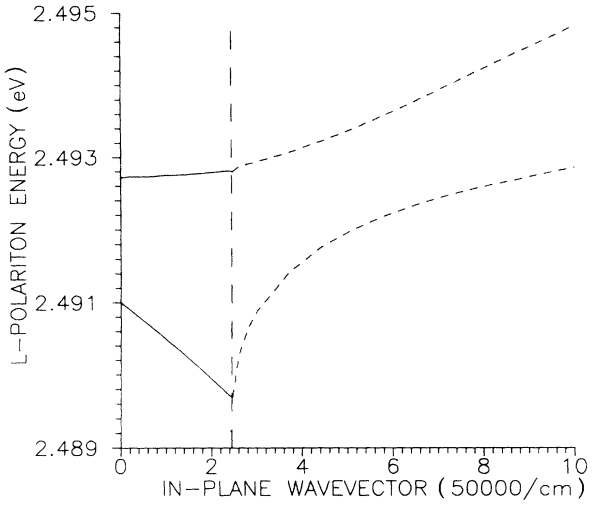

FIG. 3. Same as in Fig. 1, but with $l_1=7.1$ nm.

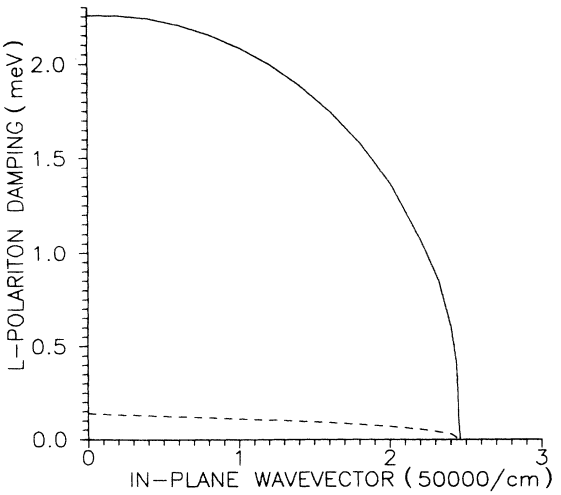

FIG. 4. Same as in Fig. 2, but with $l_1=7.1$ nm. The corresponding polaritons are in Fig. 3.

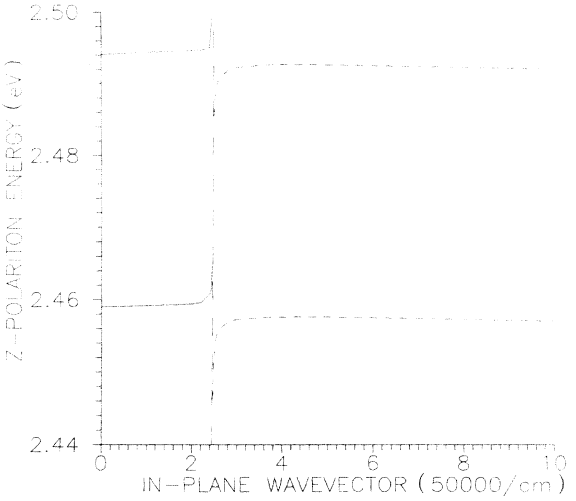

FIG. 5. Same as in Fig. 1, but for the Z polaritons.

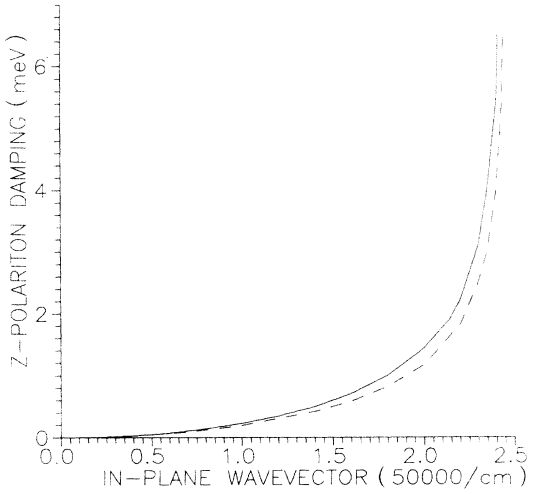

FIG. 6. Same as in Fig. 2, but for the Z polaritons in Fig. 5.

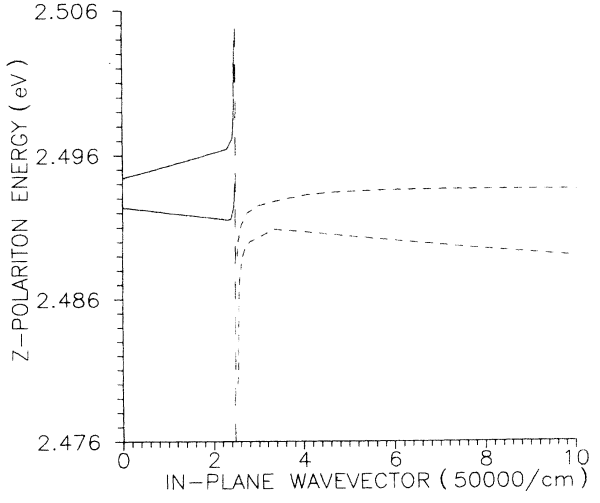

FIG. 7. Same as in Fig. 1, but with $l_1=7.1$ nm and for the Z polaritons.

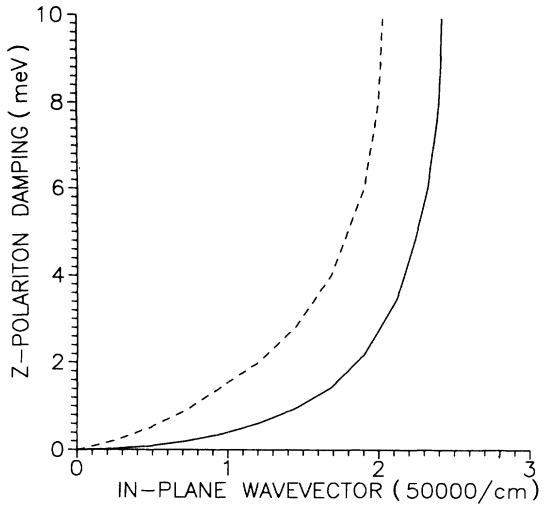

FIG. 8. Same as in Fig. 2, but with $l_1=7.1$ nm and for the Z polaritons in Fig. 7. The values of the dashed curve have been multiplied by a factor of 100.

compared to the case of uncoupled wells (in which case the two dispersions are of the same shape and just as a whole shifted from each other to different effective band gaps). The damping redistribution is more "biased": the lower polariton branch gains much more possibility for radiative decay than the upper one does (Fig. 4).

Figure 5 is the same as in Fig. 1 but for the Z polaritons. Here, at $k_\parallel=\Omega$, there is a discontinuity between damped and undamped polaritons because of the singularity in Q [see (50)] at these points. This discontinuity is associated with the impossibility to obey Maxwell boundary conditions at the barrier-well interfaces for the Z polariton (for more details see Ref. 25, which discusses this peculiarity for a SQWS). Due to the said singularity in Q, the damping for Z polaritons diverges at $k_\parallel=\Omega$ (Fig. 6). At $k_\parallel=0$ the Z-polariton damping vanishes since for these polaritons, $k_\parallel$ is a measure of photon-exciton interaction, as seen from (48). When the well width difference decreases, the dispersion reconstruction and damping redistribution become drastic for the Z polaritons, too (Figs. 7 and 8).

IV. DEPHASING BY PHONONS

The radiative decay mechanism is independent of temperature and thus is the main mechanism of polariton decay at low temperature. Only polaritons with $k_\parallel<\Omega$ can decay radiatively. So, any process scattering the polaritons into the region of $k_\parallel>\Omega$ quenches the polariton radiative decay. At high temperature the decay is influenced by phonon scattering that destroys the phase of the initial polariton. Therefore, there exists a crossover temperature T_c above which the scattering by phonons is predominant over the radiative decay process.

The polariton-phonon interaction in a coupled MQWS can be derived from the carrier-phonon one in three steps: (i) Applying the excitonization procedure, (ii) going to true excitons and, (iii) transforming to polaritons. Step (i) leads to

$$H'_{\rm int}=\sum_{\mathbf{k}_\parallel\mathbf{q}_\parallel q_\perp}\sum_{nj}M_n^{(j)}(q_\parallel,q_\perp)P^+_{n\mathbf{k}_\parallel+\mathbf{q}_\parallel}P_{n\mathbf{k}_\parallel}[a^{(j)}_{\mathbf{q}}+a^{(j)+}_{-\mathbf{q}}]\ , \tag{54}$$

where j labels the phonon modes described by the operators $a^{(j)}_{\mathbf{q}},a^{(j)+}_{-\mathbf{q}}$, which may be of bulk or confined type.[33–35] In (54) the matrix element

$$M_n^{(\rm LA)}(q_\parallel,q_\perp)=\left[\frac{q}{2\rho v L_xL_yL_x}\right]^{1/2}G_n(q_\perp)\times[Y(-\eta_h q_\parallel)D_e-Y(\eta_e q_\parallel)D_h] \tag{55}$$

is of deformation potential type for the longitudinal acoustic (L A) phonon mode with ρ being the mass density, v the sound velocity, D_e (D_h) the electron (hole) deformation potential, G_n given by (30), and

$$Y(q_\parallel)=\frac{1}{L_xL_y}\sum_{\mathbf{p}_\parallel}\chi^*(\mathbf{p}_\parallel+\mathbf{q}_\parallel)\chi(\mathbf{p}_\parallel)\ . \tag{56}$$

Casting the sum in (56) into its corresponding integral, and with $\chi(\mathbf{p}_\parallel)=\sqrt{2\pi}a_B/(1+a_B^2p_\parallel^2/4)^{3/2}$ gives

$$Y(q_\parallel)=\frac{2}{a_B^2q_\parallel^2}\left[1-\left[\frac{4-a_B^2q_\parallel^2}{4+3a_B^2q_\parallel^2}\right]^{1/2}\right]\ , \tag{57}$$

which approaches unity for $a_Bq_\parallel$ tending to zero. For the longitudinal-optical (LO) phonon mode, we use the Fröhlich interaction

$$M_n^{(\rm LO)}(q_\parallel,q_\perp)=\frac{e}{q}\left[\frac{2\pi\omega_{\rm LO}}{\epsilon^*L_xL_yL_z}\right]^{1/2}G_n(q_\perp)\times[Y(-\eta_nq_\parallel)-Y(\eta_eq_\parallel)]\ , \tag{58}$$

where $\omega_{\rm LO}$ is the frequency of a LO phonon and $1/\epsilon^*=1/\epsilon_\infty-1/\epsilon_0$ with $\epsilon_\infty(\epsilon_0)$ the high- (low-) frequency dielectric constant. For CdS $\rho=4.8$ g/cm^3, $v=5\times10^5$ cm/sec, $D_e=3.1$ eV, $D_h=-6.5$ eV, $\omega_{\rm LO}=35$ meV, $\epsilon_\infty=5.61$, and $\epsilon_0=9.35$. After steps (ii) and (iii) are performed, the polariton-phonon interaction Hamiltonian becomes

$$H'_{\rm int}=\sum_{\mathbf{k}_\parallel\mathbf{q}_\parallel q_\perp}\sum_{\alpha\beta j}\mathcal{M}^{(j)}_{\alpha\beta}(q_\parallel,q_\perp,k_\parallel,d)\mathcal{B}^+_{\alpha\mathbf{k}_\parallel+\mathbf{q}_\parallel}\times\mathcal{B}_{\beta\mathbf{k}_\parallel}[a^{(j)}_{\mathbf{q}}+a^{(j)+}_{-\mathbf{q}}]\ , \tag{59}$$

where

$$\mathcal{M}^{(j)}_{\alpha\beta}(q_\parallel,q_\perp,k_\parallel,d)=\sum_{\nu\nu'}x^*_{\nu\alpha}(k_\parallel+q_\parallel,d)x_{\nu'\beta}(k_\parallel,d)\times M^{(j)}_{\nu\nu'}(q_\parallel,q_\perp,k_\parallel,d)\ , \tag{60}$$

and

$$M^{(j)}_{\nu\nu'}(q_\parallel,q_\perp,k_\parallel,d)=\sum_n u_{n\nu}(k_\parallel+q_\parallel,d)u_{n\nu'}(k_\parallel,d)\times M_n^{(j)}(q_\parallel,q_\perp,k_\parallel)\ . \tag{61}$$

In (60) and (61), the $u_{n\nu}$ functions are determined by (24) while the $x_{\nu\alpha}$ are given by

$$x_{11}=\left|\frac{\xi_1(1-\xi_2)}{\xi_1-\xi_2}\right|^{1/2}, \tag{62}$$

$$x_{12}=-\left|\frac{\xi_2(1-\xi_1)}{\xi_2-\xi_1}\right|^{1/2}, \tag{63}$$

$$x_{22}=\left|\frac{\xi_1-1}{\xi_1-\xi_2}\right|^{1/2}, \tag{64}$$

$$x_{21}=\left|\frac{\xi_2-1}{\xi_2-\xi_1}\right|^{1/2}, \tag{65}$$

where

$$\xi_\nu\equiv\xi_\nu(p_\parallel,\Omega_\nu,d)=\left|\frac{\Omega_\nu-\mathcal{E}_2(p_\parallel,d)+R_{22}(p_\parallel,\Omega_\nu,d)}{\Omega_\nu-\mathcal{E}_1(p_\parallel,d)+R_{11}(p_\parallel,\Omega_\nu,d)}\right| . \tag{66}$$

Note that in (54) excitons before and after a scattering action remain in one and the same well, because (54) is, in fact, for uncoupled wells. If step (ii) is suppressed, i.e., if we directly approach step (iii) from step (i), we also have a picture of multibranch polariton, but interbranch transitions are prohibited, since the branches are independent in uncoupled wells. It is the Förster-type coupling that mixes the wells and makes polariton interbranch transitions allowed. In the following, we will deal with phonon-assisted dephasing of $k_\parallel=0$ L polaritons in a CdS coupled DQWS tailored as in Figs. 1 and 3. Assuming confined phonons,[20,23] the dephasing rate from the polariton $k_\parallel=0$ state on branch α to another state on branch β is evaluated as

$$\Gamma_{\alpha\beta}^{(+j)}(0)=2\pi\sum_{q_\parallel}|\mathcal{M}_{\alpha\beta}^{(j)}(q_\parallel,0,0,d)|^2[N^{(j)}(q_\parallel,T)+1]\times\delta[\Omega_\beta(q_\parallel)+\omega^{(j)}(q_\parallel)-\Omega_\alpha(0)] , \tag{67}$$

for a single-j-mode phonon emission and

$$\Gamma_{\alpha\beta}^{(-j)}(0)=2\pi\sum_{q_\parallel}|\mathcal{M}_{\alpha\beta}^{(j)}(q_\parallel,0,0,d)|^2N^{(j)}(q_\parallel,T)\times\delta[\Omega_\beta(q_\parallel)-\omega^{(j)}(q_\parallel)-\Omega_\alpha(0)] , \tag{68}$$

for a single-j-mode phonon absorption, $\omega^{(j)}(q_\parallel)=vq_\parallel$ for $j=$LA and $\omega^{(j)}(q_\parallel)=\omega_{\rm LO}$ for $j=$LO. $N^{(j)}(q_\parallel,T)$ is the Bose-Einstein distribution function for the j phonon for temperature T. In Fig. 9 the long-dashed curve is for polariton scattering from the $k_\parallel=0$ state on the upper branch ($\alpha=2$) in Fig. 1 to a $q'_\parallel$ state on the same branch ($\beta=2$) due to a single-LA-phonon emission,

$$\Gamma_{22}^{+\rm LA}(0)=0.5227[N^{\rm LA}(q'_\parallel,T)+1] \text{ meV} , \tag{69}$$

where $q'_\parallel=2.4647\times10^5$ cm^{-1} is determined from the energy conservation. The same process but due to a single-LA-phonon absorption,

$$\Gamma_{22}^{(-{\rm LA})}(0)=0.6535N^{(\rm LA)}(q'_\parallel,T) \text{ meV} , \tag{70}$$

with $q'_\parallel=2.7558\times10^5$ cm^{-1}, is represented by the short-dashed curve. The crossover temperature here is $T_c\simeq85$ K. Similar scatterings but for the structure parameters underlying Fig. 3 are depicted, respectively, by dotted and dot-dashed curves in Fig. 9. In this case, the scattered polariton lies on the lower branch ($\beta=1$):

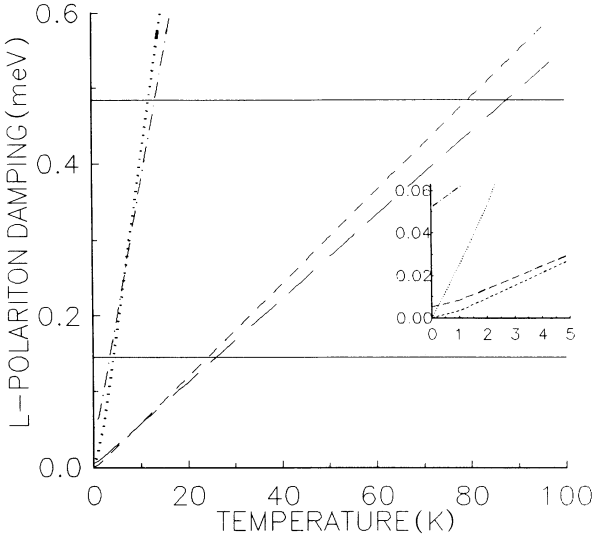

FIG. 9. Damping, in meV, of the $k_\parallel=0$ upper-branch L-polariton versus temperature, in K, for different mechanisms and well parameters. The upper horizontal line and the long-dashed (short-dashed) line represent the temperature-independent radiative decay rate and the scattering rate due to a single-LA-phonon emission (absorption) for a CdS coupled DQWS with $l_1=13$ nm, $l_2=7$ nm, and $d=10$ nm. Similar processes are, respectively, represented by the lower horizontal line and the dot-dashed (dotted) line for the same DQWS but with $l_1=7.1$ nm. The inset is the plot near the origin.

$$\Gamma_{21}^{(+{\rm LA})}(0)=0.051\,98[N^{(\rm LA)}(q'_\parallel,T)+1] \text{ meV} , \quad q'_\parallel=7.5\times10^5 \text{ cm}^{-1} , \tag{71}$$

$$\Gamma_{21}^{(-{\rm LA})}(0)=0.085\,45N^{(\rm LA)}(q'_\parallel,T) \text{ meV} , \quad q'_\parallel=1\times10^6 \text{ cm}^{-1} . \tag{72}$$

Because the radiative decay rate of the upper branch in Fig. 3 is small, T_c is only a few K. Figure 10 shows phonon-assisted dephasing of polaritons within the lower branch ($\alpha=\beta=1$). The style of dashing is the same as in Fig. 9. The long-dashed curve is due to

$$\Gamma_{11}^{(+{\rm LA})}(0)=0.002\,82[N^{(\rm LA)}(q'_\parallel,T)+1] \text{ meV} , \quad q'_\parallel=2.4647\times10^5 \text{ cm}^{-1} , \tag{73}$$

the short-dashed curve

$$\Gamma_{11}^{(-{\rm LA})}(0)=0.003\,52N^{(\rm LA)}(q'_\parallel,T) \text{ meV} , \quad q'_\parallel=2.7558\times10^5 \text{ cm}^{-1} , \tag{74}$$

the dot-dashed curve

$$\Gamma_{11}^{(+{\rm LA})}(0)=0.007\,79[N^{(\rm LA)}(q'_\parallel,T)+1] \text{ meV} , \quad q'_\parallel=1.51\times10^5 \text{ cm}^{-1} , \tag{75}$$

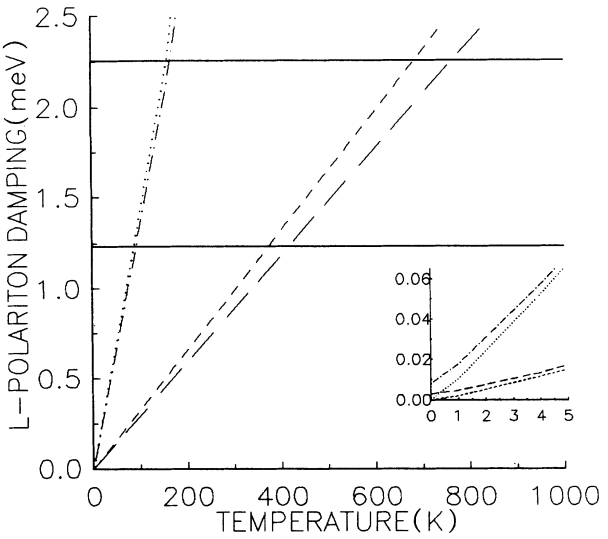

FIG. 10. Same as in Fig. 9, but of the $k_{\parallel}=0$ lower-branch L polaritons.

and, the dotted curve

$$\Gamma_{11}^{(-\mathrm{LA})}(0)=0.008\,75N^{(\mathrm{LA})}(q'_{\parallel},T)\ \mathrm{meV}\ ,$$

$$q'_{\parallel}=1.6\times10^{5}\ \mathrm{cm}^{-1}\ . \quad (76)$$

Because of the damping redistribution discussed in the previous section, the lower polariton branch has a shorter radiative lifetime than the upper one. This yields $T_c\simeq400$ K for the parameters underlying Fig. 1 and $T_c\simeq170$ K for the parameter underlying Fig. 3. A message worth noticing is that all the $q'_{\parallel}$ values evaluated above are on the rhs of the curve $\Omega=k_{\parallel}$, revealing that the scattered polariton no longer has the ability to decay radiatively. So it is difficult to observe this decay at high enough temperatures. At room temperature ($T\simeq300$ K) the radiative decay for the coupled DQWS under consideration is completely quenched by phonons, except for the decay channel from the lower branch in Fig. 3.

Concerning LO phonons, their contribution is negligible here. We have on purpose tailored the DQWS in Fig. 1 so that the polariton energy separation at $k_{\parallel}=0$ is close to ω_{LO} (here, for CdS, it is of 35 meV). In spite of that, the smallness of $q'_{\parallel}$ satisfying energy conservation makes the quantity in the square brackets in (58) very small.

V. DISCUSSION AND CONCLUSION

The polariton theory in a SQWS (Refs. 23–26) has just recently been tested experimentally[27,28] in GaAs quantum wells. Reference 27 has used time-resolved luminescence spectroscopy to measure the exciton radiative lifetime when the wells are excited in close resonance with the exciton. The fast component of the measured luminescence decay curve is interpreted as the polariton effect in the volume limited by the quantum-well size. In Ref. 28, instead, the stationary photoluminescence spectrum has been measured at different angles of incidence of the exciting laser beam, which is then fit theoretically by using analytic expressions for polariton radiative damping in a simple model of rate equations. As the authors claim, their observation is the first, though indirect, experimental confirmation of the finite polariton radiative lifetime in a uncoupled MQWS. No attention has been drawn to interwell coupling in the above experiments. To the best of our knowledge, no theory has dealt with polaritons in coupled MQWS's as yet. The interwell coupling, as we discussed in our paper, would lead to a branch-dependent damping rate.

Optical excitation of a coupled MQWS generates the polaritons which do not belong to any individual well but are characteristic of the whole coupled structure. In a coupled DQWS, say, there are two-polariton branches: the upper and the lower one. Here, one can by no means say that the upper branch is narrow-well-like and the lower one is wide-well-like because it turns out to be wrong in the case of two identical wells (i.e., a symmetric DQWS) where two distinct true excitons appear[20] and thus two distinct polariton branches result, though the two wells are indistinguishable. Since interwell coupling allows polariton interbranch transition, when a given branch is excited, one could observe luminescence from another branch which has not directly been excited or, one could also expect the Stokes/anti-Stokes line resulting from Raman scattering due to a polariton interbranch jumping. Such effects are a manifestation of energy transfer in a MQWS via a dipole-dipole exciton-exciton interaction in different wells. Recently, the authors of Refs. 15 and 17 have reported on observations of energy transfer between quantum wells separated by a thick barrier which, as they claim with a question mark, should be due to the Föster-type coupling mechanism. We do not attempt to explain this experiment because this scenario is still quite unclear especially with respect to the reported independence of both temperature and barrier thickness. We would just like to say that the polariton approach should be appropriate and the barrier-temperature dependence should be somehow displayed. This is because the barrier thickness enters explicitly in the hopping strength and, when the wells are not biased by an applied field to align the energy sublevels in separate wells, the polariton interbranch transition energy conservation would most likely require phonon participation, which gives rise to a temperature dependence. Is it conceivable that the energy-transfer process observed in Refs. 15 and 17 is caused by another mechanism not yet identified at present?

In conclusion, we have theoretically developed a picture of polaritons in a coupled MQWS, when tunneling is ignored. The interwell coupling considered here is of the Förster type, which occurs via the dipole-dipole exciton-exciton interaction in different wells. This exciton-exciton coupling, in turn, originates from the long-range electron-hole exchange interaction. As an example, we have carried out numerical calculation in the case of a CdS coupled DQWS for the dependence of both polariton energy and radiative damping on the in-plane wave vector. The calculated results have shown interesting features as compared to the uncoupled wells case.

ACKNOWLEDGMENTS

We wish to thank Professor P. Thomas for communications on the topic and for making Ref. 17 available to us prior to publication. This work has been supported by the Stuttgart Max-Planck Institute for Solid State Physics and the Institute for Theoretical Physics and Synergetics of the University of Stuttgart, Germany.

---

*Permanent address: Institute of Physics, P.O. Box 429 Boho, Hanoi 10000, Vietnam.

[1]S. Scandolo and F. Tassone, Phys. Status Solidi B **173**, 453 (1992).

[2]Hartmut G. Roskos, Martin C. Nuss, Jagdeep Shah, Karl Leo, David A. B. Miller, A. Mark Fox, Stefan Schmitt-Rink, and Klaus Köhler, Phys. Rev. Lett. **68**, 2216 (1992).

[3]V. May, O. Kühn, P. Thomas, and H. Vaupel, Phys. Status Solidi B **177**, 175 (1993).

[4]H. Cruz, A. Hernández-Cabrera, and P. Aceituno, Solid State Commun. **90**, 515 (1994).

[5]E. Binder, T. Kuhn, and G. Mahler, Phys. Rev. B (to be published).

[6]T. Kuhn and G. Mahler, Solid-State Electron. **32**, 1851 (1989).

[7]G. Bacher, C. Hartmann, H. Schweizer, T. Held, G. Mahler, and H. Nickel, Phys. Rev. B **47**, 9545 (1993).

[8]S. V. Railson, D. Wolverson, J. J. Davies, D. Ashenford, and B. Lunn, Superlatt. Microstruct. **13**, 487 (1993).

[9]Nanzhi Zou, K. A. Chao, and Yu. M. Galperin, Phys. Rev. Lett. **71**, (1993).

[10]F. T. Vasko, O. G. Balev, and P. Vasilopoulos, Phys. Rev. B **47**, 16 433 (1993).

[11]T. B. Norris, N. Vodjdani, B. Vinter, E. Costard, and E. Böckenhoff, Phys. Rev. B **43**, 1867 (1991).

[12]A. M. Fox, D. A. B. Miller, G. Livescu, J. E. Cunningham, and W. Y. Jan, Phys. Rev. B **44**, 6231 (1991).

[13]B. Deveaud, A. Chomette, B. Lambert, A. Regreny, R. Romestain, and P. Edel, Solid State Commun. **57**, 885 (1986).

[14]A. Nakamura, N. Kawamoto, K. Fujiwava, N. Tsukoda, and T. Kawamoto, Solid State Commun. **71**, 553 (1989).

[15]A. Tomita, J. Shah, D. S. Kim, T. C. Damen, J. M. Kuo, S. Schmitt-Rink, P. Thomas, and R. S. Knox, Int. Conf. Quantum Electron. Tech. Digest, Ser. **9**, 102 (1992).

[16]Leonid G. Gerchikov and Arsen V. Subashiev, Solid State Commun. **90**, 57 (1994).

[17]A. Tomita, J. Shah, D. S. Kim, T. C. Damen, J. M. Kuo, S. Schmitt-Rink, P. Thomas, and R. S. Knox (unpublished).

[18]Th. Förster, Ann. Phys. (Leipzig) **2**, 55 (1948).

[19]Bing Shen Wang and Joseph L. Birman, Phys. Rev. B **43**, 12 458 (1991).

[20]M. Batsch, T. Meier, P. Thomas, M. Lindberg, S. W. Koch, and J. Shah, Phys. Rev. B **48**, 11 817 (1993).

[21]A. S. Davydov, *Theory of Molecular Excitons* (Plenum, New York, 1971).

[22]J. J. Hopfield, Phys. Rev. **112**, 1555 (1958).

[23]Eiichi Hanamura, Phys. Rev. B **38**, 1228 (1988).

[24]Lucio Claudio Andreani and Franco Bassani, Phys. Rev. B **41**, 7536 (1990).

[25]F. Tassone, F. Bassani, and L. C. Andreani, Nuovo Cimento **12**, 1673 (1990).

[26]F. Tassone, F. Bassani, and L. C. Andreani, Phys. Rev. B **45**, 6023 (1992).

[27]B. Sermage, B. Devead, K. Satzke, F. Clérot, C. Dumas, N. Roy, D. S. Katzer, F. Mollot, R. Planel, M. Berz, and J. L. Oudar, Superlatt. Microstruct. **13**, 271 (1993).

[28]Victor Pellegrini, Francesco Fuso, and Ennio Arimondo, Solid State Commun. **90**, 167 (1994).

[29]H. Haug and S. Schmitt-Rink, Quantum Electron. **9**, 3 (1994).

[30]Nguyen Ba An, Hoang Ngoc Cam, and Nguyen Trung Dan, J. Phys. Condens. Matter **3**, 3317 (1991).

[31]A. L. Ivanov and H. Haug, Phys. B **48**, 1490 (1993).

[32]R. Ferreira, P. Rolland, Ph. Roussignol, C. Delalande, A. Vinattieri, L. Carraresi, M. Colocci, N. Roy, B. Sermage, and J. F. Palmier, Phys. Rev. B **45**, 11 782 (1992).

[33]G. Mahler, A. M. Kriman, and D. K. Ferry, in *OSA Proceedings on Picosecond Electronics and Optoelectrons,* edited by T. C. L. Gerhard Sollna and David M. Bloom (Optical Society of America, Washington, D.C., 1989), Vol. 4, p. 163.

[34]Nguyen Van Trong, G. Mahler, and A. Fourikis, Phys. Rev. B **38**, 7674 (1988).

[35]J. S. Bhat, B. G. Mulimani, and Kubakaddi, Phys. Status Solidi B **182**, 119 (1994).